J Mater Sci (2008) 43:5342–5349
DOI 10.1007/s10853-008-2781-0

Viscoplastic behaviour of metals deformed at high-temperature, application to tension–compression cycles

Vladimir Gantchenko · Patrice Jouinot · Alain Köster

Received: 8 November 2007 / Accepted: 5 June 2008 / Published online: 24 June 2008
© Springer Science+Business Media, LLC 2008

Abstract A mechanical modelling is proposed in order to describe viscoplastic behaviour without hardening of a nickel-base super alloy loaded at high temperature (900 °C) with strain rates varying within a wide range (from 10^{-1} to 10^{-4} s^{-1}). A mathematical law is associated to the viscoplastic model; the parameters of the law are identified from monotonic biaxial tests of membranes loaded by pressure of inert gas (disk pressure testing under helium). The viscoplastic law provides calculated stresses with accuracy better than 1% at the highest strain rates and 4% at the lowest strain rates; the identified yield stress is a logarithmical function of strain rate as for other metallic alloys studied in the bibliography. The parameters identified from biaxial tensile tests of disks have been successfully used to calculate the stresses during stabilized tension–compression loops of cylindrical specimens. The proposed experimental method and behaviour model are interesting because the disk biaxial testing is much more easily performed at high temperature than the tension–compression testing of cylindrical specimens.

Introduction

The mechanical properties of Inconel 600 have been measured within a wide range of temperatures and within a wide range of loading rates in order to identify the behaviour of this material subject to extreme thermo-mechanical loading; in this article, a mathematic model is proposed for Inconel 600 mechanically loaded at 900 °C (1173 K) with various strain rates. As the test temperature is about 70% of absolute melting temperature, the material behaviour is viscoplastic without hardening by mechanical deformation such as in a cold-working.

The model and its parameters have been identified by monotonic bulging testing: a thin disk is deformed by a continuously increasing pressure of inert gas (helium) until its final rupture [1]. The bulging tests can be performed at strain rates within ranges much wider than ranges usually obtained with a single type of specimen and with a single mechanical testing machine [2]. The proposed model and the identified parameters have been used to characterize the same material during tension–compression cycles after stress stabilization in order to evaluate their efficiency and accuracy.

Interest of disk testing and its associated modelling

The usual sample and equipment for tension–compression cycles are schematised in the Fig. 1; the sample must be confined in an atmosphere of inert gas to avoid its oxidization [3]. However, the results obtained with a tensile specimen at high temperature (900 °C or higher for Inconel 600) may not be used if the sample axis does not coincide perfectly with the tensile machine axis; because of this geometrical imperfection, the sample compression initiates buckling during the first cycles with the result that the sample is not homogeneously deformed; moreover, the local plastic strain amplifies the specimen deformation initiated by buckling.

During disk pressure testing, the material is only loaded by tension stresses; so, buckling does not occur as during

V. Gantchenko (✉) · P. Jouinot
ISMEP, 93407 Saint Ouen, France
e-mail: gantchenko@supmeca.fr

A. Köster
ENSMP, 91003 Evry, France

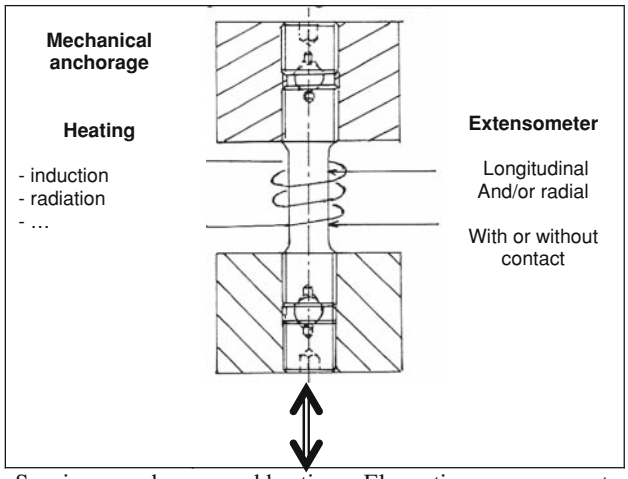

Fig. 1 Schematic equipment for tension–compression testing at high temperature

the compression phases of the alternately cyclic loading of the tensile specimen. If modelling from disk pressure testing is sufficiently efficient and accurate, it can be used to determine the stresses during the stabilized cycles of tension–compression at high temperature.

Another interest of disk testing is temperature homogeneity: the temperature gradient is low in the deformed zone of thin disk (1 mm) tested at elevated temperature; for the relatively long samples of tension–compression heated by radiation or induction, the thermal gradient is higher because of the thermal flow through the clamping equipment. Moreover, biaxial testing of disks is much more easily performed than tension–compression cycles or than a classical tensile test at high temperature; besides, during disk testing, material damage may be identified when fine and short cracks create helium leakages through the deformed disk; helium leakages are sensitively detected by a mass spectrometer analysing the atmosphere above the disk [4].

Material

Inconel 600 is a nickel super-alloy with chromium (14–17%) and iron (6–10%); the melting temperature of Inconel 600 is in the range of 1350–1410 °C. This alloy has good high temperature strength up to 1150 °C and it resists chemical corrosion at high temperatures. For high-temperature engineering, the alloy displays good resistance to oxidation and carburisation [5]. As a result of its versatility, Inconel 600 finds a variety of applications with severe thermo-mechanical and chemical conditions: chemical industry, aeronautical and space fields, nuclear reactors….

Experimental technique

Biaxial testing of disks

During biaxial testing, a thin disk is deformed into a cupola by a continuously increasing pressure of helium up to final rupture (Fig. 2). The geometry of the cell and sample has been determined in order to calculate more easily the strains and stresses at the cupola pole. During the monotonic testing, several parameters are plotted until disk rupture: the gas pressure applied to the disk face, the deflection of the disk pole, the disk temperature, the flow of helium leakage through the disk resulting from material damage.

The cell and the disk may be heated with an annular furnace; the temperature is measured by a thermocouple in contact with the disk upper face. The temperature is quasi homogeneous in the thin disk confined in the thermally correctly insulated cell. Before disk loading, heating duration takes about 1 h; when the material must be tested at high temperature, lengthy heating duration may create substantial evolutions to the metallurgical structure of the material. A mass spectrometer measures gas flow through the disk; it detects crossing cracks (generally inter-granular) that have been developed before the final rupture. These fine and relatively short cracks do not modify the global mechanical behaviour of the disk [6].

During testing, the disk periphery is not mechanically loaded with the result that machining defects do not initiate area reductions such as in tensile specimens especially when they are tested at high temperature.

Mechanical properties of the disk

An analytical calculation similar to Hill's method [7] is used to calculate the plastic strain and stress at the disk pole from the measured deflection and pressure [1, 4]. The calculation

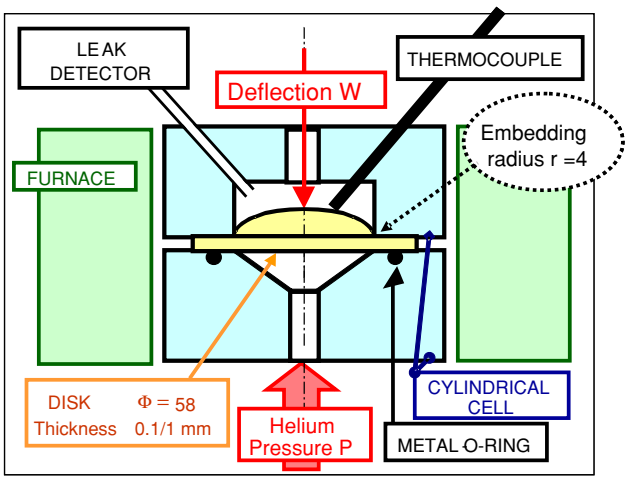

Fig. 2 Cell of disk pressure testing

of plastic strains and stresses is based on the following assumptions: the stresses are biaxial because the maximum axial stress is the gas pressure that is negligible in comparison to plane stresses; the material is homogeneous, isotropic and the volume of a metallic material is constant during plastic deformation; the thin disk is deformed as a membrane, i.e. the flexion is neglected at the pole.

The most general mechanical loading corresponds to six independent parameters, three principal stresses and three principal strains. For the disk loading, the axial stress is nullified; the Von Mises stress and strain are calculated from the five remaining parameters in order to compare the results of disk testing and tensile testing. Obviously, the Von Mises stress and strain are restrictive because only two parameters describe the disk behaviour instead of the five initial parameters; however, the restrictive Von Mises stress and strain have provided coherent comparisons of different mechanical loadings in many applications [8–11]. The Von Mises stress $\bar{\sigma}$ and strain $\bar{\varepsilon}$ are determined from the Eqs. 1 and 2,

$$\bar{\sigma} = \frac{P\rho}{2t} \tag{1}$$

$$\bar{\varepsilon} = \ln(t_0/t) \tag{2}$$

where P is the gas pressure, ρ the cupola radius at the disk pole, t the pole thickness of the deformed disk and t_0 the initial thickness of the disk.

If the deformed disk is assumed to be a spherical cupola, the pole radius ρ is the sphere radius; this radius is determined from the deflection W by the geometrical relation (3) obtained for the outer fibre of the disk (Fig. 3). We have verified by dimensional measurements that the disk is deformed into the assumed spherical cupola,

$$\rho = (W^2 + A^2)/(2W) - r \tag{3}$$

where W is the deflection at the disk pole, A the internal radius of the disk embedding and r the die radius at the disk embedding.

The strains at the disk pole are calculated from the deflection W by the analytic formula (4) based on the abovementioned assumptions; this formula has been validated by measurements of the pole thickness obtained after deformation of disks made of various materials,

$$\bar{\varepsilon}_i = 2\int_0^{W_i} \frac{\left[1 - \frac{2r}{A}\left(\frac{1}{1+\frac{W^2}{A^2}}\right)\sin\left(2\mathrm{Ar}\tan\left(\frac{W}{A}\right)\right)\right]}{\rho} \mathrm{d}W \tag{4}$$

where W is the deflection at the disk pole, A the internal radius of the disk embedding, r the die radius at the disk embedding and ρ the radius of the disk deformed as a spherical cupola; the radius ρ is calculated from the deflection with the formula (3).

Disk testing associated to the previous calculation method provides coherent mechanical properties, similar to the usual tensile mechanical properties: the ultimate strength and the proof strength are identical if they are determined by disk testing or by tensile testing (Figs. 4 and 5); the mean values of the uniform elongation are identical for the both testing methods but the scattering is relatively more important than

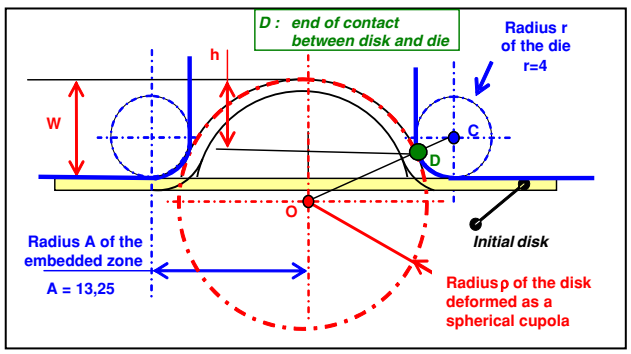

Fig. 3 Disk deformation: geometrical parameters

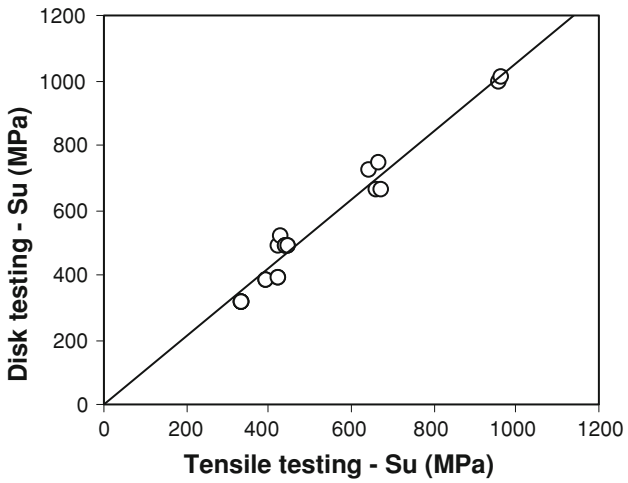

Fig. 4 Ultimate strength Su: disk and tensile testing

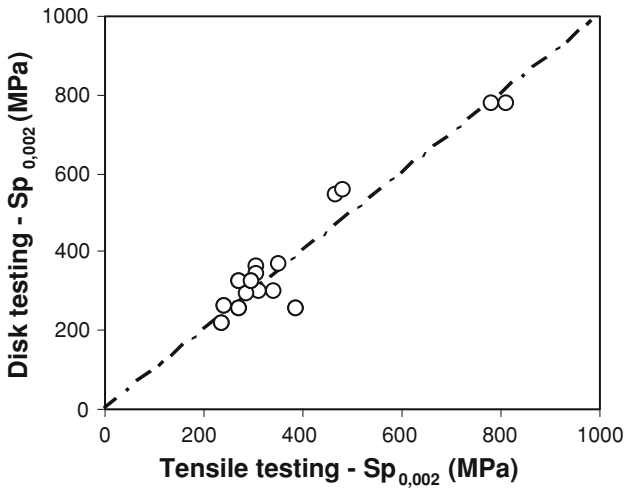

Fig. 5 Proof strength $Sp_{0,002}$: disk and tensile testing

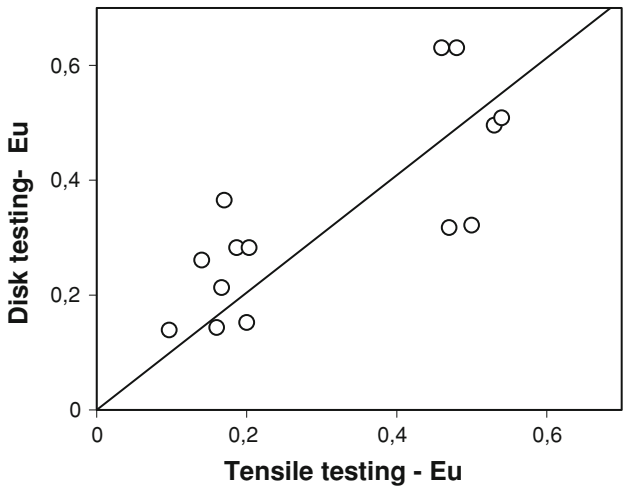

Fig. 6 Uniform elongation Eu: disk and tensile testing

the strength scattering (Fig. 6). The elongation scattering depends on local deformations initiated by the material heterogeneities (surface defects as machining defects, metallurgical defects as coarse inclusions…); the material heterogeneities initiate area reductions that are not detected with the same sensitivity for a thick tensile specimen or for a thin disk. Besides, the outer disk periphery is not stressed with the result that the area reduction cannot be initiated on the edge defects as for the tensile specimen.

The mechanical properties are correctly related to phenomena depending on temperature and loading rate (Fig. 7): at the highest temperatures, low-alloyed steel strength decreases because the material is dynamically re-crystallized during a deformation at high temperature; at intermediate temperatures, the material is hardened by a phenomenon related to the solute atoms; hardening is more important for disk testing than for tensile testing because the strain rate, an important factor of hardening, is not identical for both specimens.

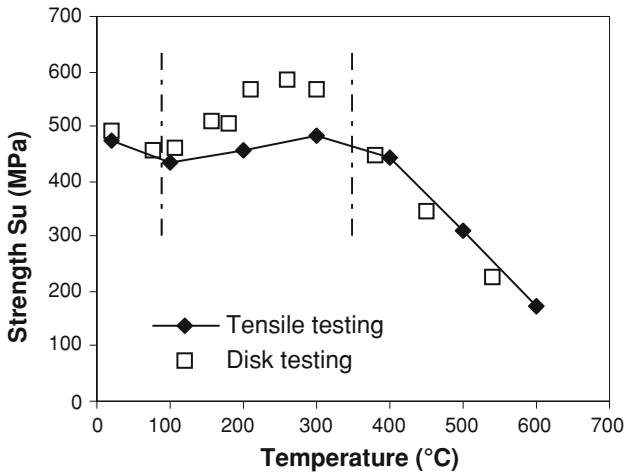

Fig. 7 Influence of temperature on the ultimate strength Su: disk and tensile testing

The biaxial tests can be performed at temperatures between 20 and 900 °C and at strain rates between 10^{-6} and 10^{0} s^{-1}; for instance, tests can be performed at 900 °C at high strain rate [2], which is difficult with another experimental technique. The previous results evidence coherent comparisons between disk testing and tensile testing; as for other applications, the Von Mises stress and strain are sufficient to obtain coherent comparisons while they restrict the initial set of six stresses and strains to only two parameters.

Experimental results

Biaxial tests have been performed at 900 °C with disks made of as-received Inconel 600; disks have been cut from a 0.6-mm-thick sheet; before mechanical stressing, the heating duration needs about 1.5 h and a wide range of pressure rates has been tested (3×10^{-2} to 3×10^{1} MPa/s). The disk rupture needs about 6 min at 3×10^{-2} MPa/s and about 1 s at 3×10^{1} MPa/s. The rupture pressure remains relatively small at low pressure rate (10.6 MPa at 3×10^{-2} MPa/s), while it is three times higher at high strain rate (31 MPa at 3×10^{1} MPa/s).

Von Mises stresses, Von Mises plastic strains and strain rates have been calculated with the described method from the measured pressure and deflection (Fig. 8). Obviously, the range of strain rates (from 3.31×10^{-4} to 2.37×10^{-1} s^{-1}) is as wide as the range of pressure rates. For a defined strain, the stress strongly increases when the strain rate increases; for instance, when the plastic strain is nullified, the stress increases from 100 MPa at 3.31×10^{-4} up to 300 MPa at 2.37×10^{-1} s^{-1}; the influence of the material viscosity is very important because the testing temperature is high relatively to the melting temperature of Inconel 600.

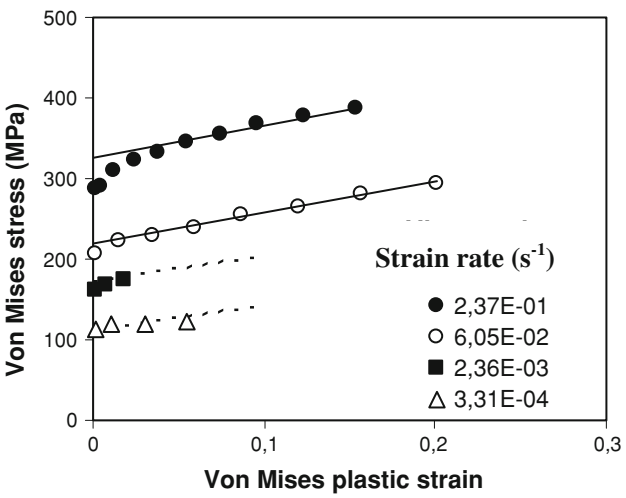

Fig. 8 Measured stresses and strains

For the lowest strain rates ($\dot{\varepsilon} \leq 2.36 \times 10^{-3}\ s^{-1}$), the maximum uniform strains are relatively small ($\varepsilon < 6\%$) because cracks are initiated on the coarse precipitates created by thermal ageing at 900 °C; the cracks propagate through the whole disk thickness and prevent further pressurisation. For the highest strain rates ($\dot{\varepsilon} \geq 6.05 \times 10^{-2}\ s^{-1}$), the test duration is too short to obtain the coarse precipitates by thermal ageing; consequently, the disk can be pressurised up to relatively high uniform deformations ($\varepsilon > 15\%$). At the two highest strain rates ($\dot{\varepsilon} = 6.05 \times 10^{-2}\ s^{-1}$ and $\dot{\varepsilon} = 2.37 \times 10^{-1}\ s^{-1}$), the stress–strain curves reach linear and parallel asymptotes; we assume that similar parallel asymptotes could be reached at the lowest strain rates ($\dot{\varepsilon} = 3.31 \times 10^{-4}\ s^{-1}$ and $\dot{\varepsilon} = 2.36 \times 10^{-3}\ s^{-1}$) if cracks had not been propagated through the disk thickness.

In conclusion, we assume that material plastic behaviour is linear for the highest plastic strains at any rate; the linear behaviour will be described by asymptotes with a common slope at any strain rate.

Modelling the monotonic mechanical behaviour at 900 °C

Mechanical model

The mechanical behaviour of Inconel 600 at 900 °C may be described by a tripartite model (Fig. 9).

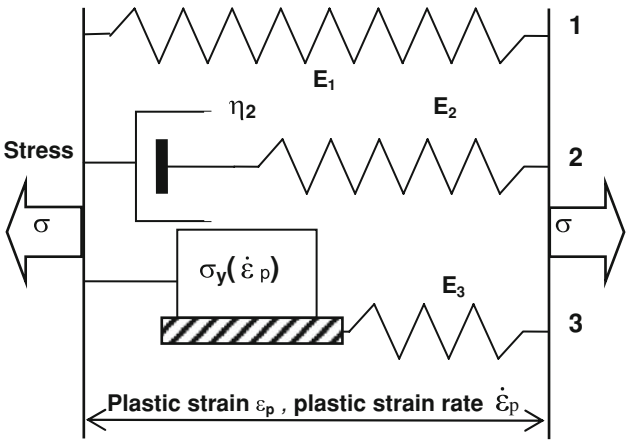

1 : Linear behavior at high ε_p
Spring of modulus E_1
2 : Viscoplastic behavior at low high ε_p
Damper of viscosity η_2
Spring of modulus E_2
3 : Rigid and perfectly plastic solid
Plastic deformation from $\sigma_y(\dot{\varepsilon}_p)$
Elasticity: spring of modulus E_3

Fig. 9 Mechanical viscoplastic tripartite model

1. The spring of modulus E_1 characterises the linear mechanical behaviour at the highest plastic strains; the modulus E_1 is the common slope of the linear and parallel asymptotes.
2. The spring of modulus E_2 and the damper η_2 characterize the material viscoplasticity for the lowest plastic strains.
3. The third spring of modulus E_3, added to the springs E_1 and E_2, describes the elastic behaviour; as the disk testing only provides the plastic strain, the modulus E_3 has to be measured by another technique. The deformation becomes plastic when the stress reaches the yield stress σ_y; the value of the stress σ_y depends on the plastic strain rate $\dot{\varepsilon}_p$.

Viscoplastic law describing to the proposed model

According to the proposed model, the viscoplastic tensile behaviour of Inconel 600 is described by Eq. 5:

$$\sigma(\varepsilon_p, \dot{\varepsilon}_p) = E_1\varepsilon_p + \eta_2\dot{\varepsilon}_p\left[1 - \exp\left(-\frac{E_2\varepsilon_p}{\eta_2\dot{\varepsilon}_p}\right)\right] + \sigma_y(\dot{\varepsilon}_p) \tag{5}$$

When the plastic strain ε_p is sufficiently high, the stress reaches a linear asymptote described by Eq. 6:

$$\begin{aligned}\sigma(\infty, \dot{\varepsilon}_p) &= E_1\varepsilon_p + \eta_2\dot{\varepsilon}_p + \sigma_y(\dot{\varepsilon}_p)\\ \sigma(\infty, \dot{\varepsilon}_p) &= a_1\varepsilon_p + b_1\end{aligned} \tag{6}$$

The parameters of the asymptote equation, $a_1(\dot{\varepsilon}_p) = E_1$ and $b_1(\dot{\varepsilon}_p) = \eta_2\dot{\varepsilon}_p + \sigma_y(\dot{\varepsilon}_p)$ are determined by linear fitting of the experimental results obtained at the highest strains ε_p; these parameters may depend on the strain rate $\dot{\varepsilon}_p$. As the linear asymptotes are parallel, a single value of the modulus E_1 is expected; this single value is the mean value calculated from the tests at the both highest strains. At the lowest strain rates, asymptotes are adjusted by extrapolation at high strain; the asymptotes slope is the prior mean value of the modulus E_1; consequently, the parameter b_1, obtained by nullifying the strain in the asymptote equation, can also be determined for the low strain rates.

For each test, the linear asymptotes are extrapolated down to the smallest strains; from this extrapolation, we can determine the difference D between the measured stress and the asymptotic stress calculated by Eq. 6; the difference D corresponds to Eq. 7.

$$\begin{aligned}D(\varepsilon_p, \dot{\varepsilon}_p) &= \eta_2\dot{\varepsilon}_p \exp\left(-\frac{E_2\varepsilon_p}{\eta_2\dot{\varepsilon}_p}\right)\\ D(\varepsilon_p, \dot{\varepsilon}_p) &= b_2 \exp(-a_2\varepsilon_p)\end{aligned} \tag{7}$$

The coefficients $a_2(\dot{\varepsilon}_p) = E_2/\eta_2\dot{\varepsilon}_p$ and $b_2(\dot{\varepsilon}_p) = \eta_2\dot{\varepsilon}_p$ are determined by exponential fitting of the difference D as a

function of the strain ε_p; these coefficients depend on the strain rate $\dot{\varepsilon}_p$.

Finally, all the parameters of the behaviour law (5) are identified from disk tests performed at different strain rates $\dot{\varepsilon}_p$: the modulus E_1 is the slope a_1 obtained for the stress–strain curves at the both highest strain rates $\dot{\varepsilon}_p$; the damping η_2 is calculated from the coefficient b_2 and from the strain rate for each test; the modulus E_2 is calculated from the coefficient a_2, the strain rate $\dot{\varepsilon}_p$ and the damping η_2; the yield strength σ_y is calculated at each strain rate from the coefficient b_1 and the damping η_2 while the b_1 value is obtained by Eq. 6 of the asymptotes reached at the highest strains.

Viscoplastic parameters identified for Inconel 600 at 900 °C

The modulus at highest plastic strains has been determined with accuracy better than 2% for both the highest strain rates: $E_1 = 371$ MPa. The modulus and viscosity at lowest plastic strains have been determined with accuracy better than 2% for the different strain rates: $E_2 = 1642$ MPa and $\eta_2 = 229$ MPa s. The yield stress σ_y depends on the plastic strain rate (Fig. 10).

Influence of strain rate on the yield stress

The yield stress σ_y logarithmically increases as a function of the plastic strain rate $\dot{\varepsilon}_p$ (Fig. 11); identical results have been obtained with low carbon steels [12–14], molybdenum [15]. This logarithmic increase of the yield stress σ_y induces the exponential law (8) giving the strain rate as a function of the stress; this law has already been obtained for crystallized solids loaded by high stresses at high temperatures [16].

$$\sigma_y = A \ln(\dot{\varepsilon}_p) + B \Rightarrow \dot{\varepsilon}_p = C \exp(\sigma_y/\sigma_0) \quad (8)$$

Accuracy of the proposed model

For each strain and each strain rate, the stresses at the disk pole have been calculated by using the proposed model and the previously identified parameters. The calculated stresses are compared to the measured stresses (Fig. 12); the behaviour modelling and the identified values of the parameters are correct because the accuracy between the calculated and the measured stresses is better than 1% for the highest strain rates; for the lowest strain rates, the accuracy remains better than 4%.

Plastic strain rate (s^{-1})	Yield stress (MPa)
3.31E-04	109
2.36E-03	158
6.05E-02	204
2.37E-01	282

Fig. 10 Identified yield stress versus plastic deformation rate

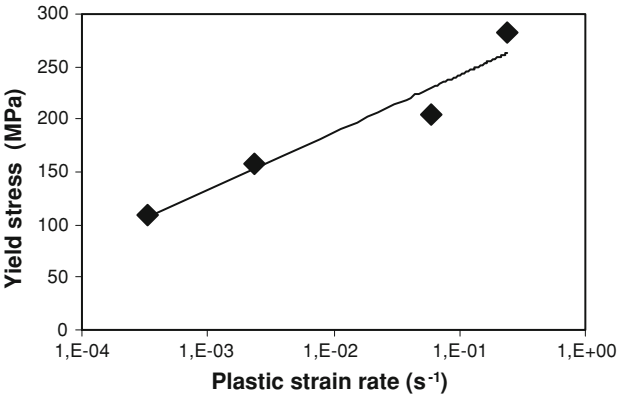

Fig. 11 Influence of plastic strain rate on yield stress

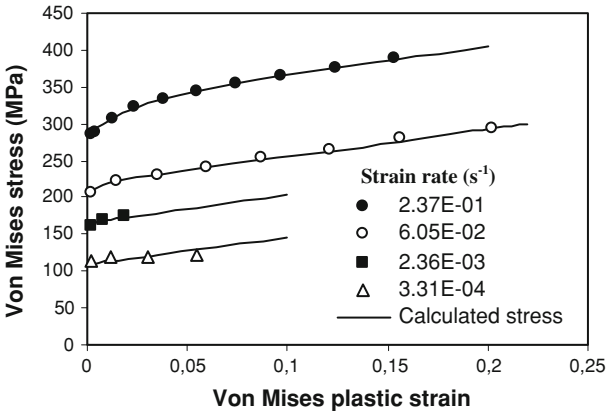

Fig. 12 Comparison of the calculated and measured stresses

Application of the model reliability to uniaxial compression–tension cycles

The abovementioned viscoplastic model has been used to calculate stress during uniaxial compression–tension cycles at total extreme strains of ±1% when the cyclic hardening has been stabilized; the evolution of the imposed strain is shown in Fig. 13a. The same value of the yield stress σ_y has been used for tension loading and compression loading and the elastic modulus has been determined by tensile testing at high temperature.

The calculated stresses are similar to the measured stresses (Fig. 13b) despite the differences between the tested materials and specimens: the calculated stresses have been obtained from the prior tripartite model and from the associated behaviour law; the needed parameters have been

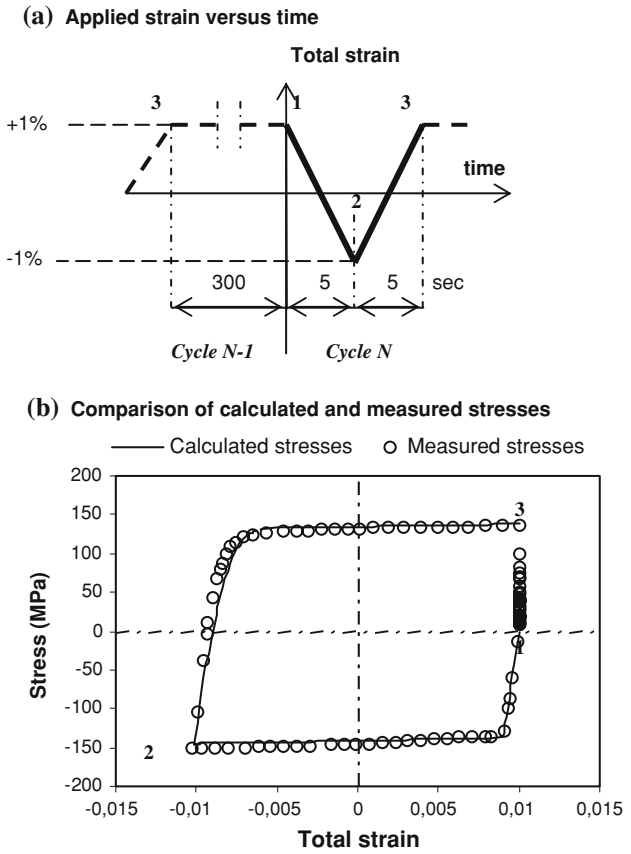

Fig. 13 Calculated and measured stresses during compression–tension cycles

identified by ISMEP's laboratory from biaxial testing of disks loaded by gaseous pressure while the experimental compression–tension stresses have been measured by ENSMP with cylindrical specimens machined from bars; the disks have been cut off from thin plates and the cylindrical specimens have been machined from extruded bars made of the same standardized alloy but the plates and the bars have been separately prepared.

Discussion

Different models are used to simulate the mechanical behaviour of metals; the basic multiplicative model $(\sigma(\varepsilon_p, \dot{\varepsilon}_p) = \sigma_0 \varepsilon_p^n \dot{\varepsilon}_p^m)$ is derived from Hollomon's law and needs only three parameters; the multiplicative model is not as precise as our model, especially if the ranges of strains and strain rates are very wide. Other numerical models are proposed for modelling the metal behaviour, particularly at high temperature. For instance, the mechanical behaviour of metals may be simulated by Lemaitre-Chaboche's model; the five coefficients of stabilized cycles modelling have been identified at different temperatures for several materials and particularly for Inconel [17]. Lemaitre-Chaboche's model has been successfully used in order to simulate the mechanical behaviour of disks made of copper alloy [18], but this numerical model does not seem to simulate every phase of mechanical cycles after stabilization as perfectly as our proposed model [19]. Our viscoplastic modelling has been successfully used for determining the behaviour of low-alloyed copper tested at 65% of its absolute melting temperature and at strain rates within ranges as wide for Inconel 600.

The logarithmic relation between the yield stress and the strain rate may be attributed to the following physical mechanism: the plastic strain is controlled by the creation of mobile dislocations slipping among the forest of immobile dislocations [20, 21]. The other parameters of our analogical model, modulus and damping, are not related to physical mechanisms; they are identified from the behaviour of basic mechanical components; this concrete approach is interesting because it is didactic to evidence different phenomena and to evaluate the influence of factors as temperature. The numerical models, as Hollomon's model or Lemaitre-Chaboche's model, are used to describe phenomena revealed by experimental results; generally, the numerical models are not based on a concrete significance with the result that they are not as didactic as the proposed analogical model.

Conclusion

At 900 °C, Inconel 600 is not hardened by mechanical deformation; its behaviour is linear for the highest strains. The proposed viscoplastic model is reliable and versatile; this model and the parameters have been identified from disks bulged by continuously increasing pressure and they provide accurate stresses for compression–tension cycles of uniaxial specimens loaded up to imposed maximum strain. However, disk testing is much more easily performed than compression–tension cycles at high temperature.

The proposed model provides parameters related to basic mechanical behaviours contrary to numerical models; this concrete approach is useful to understand the phenomena and their modifications by different factors. The proposed testing and modelling provide results related to physical mechanisms described in the bibliography as the dislocation mobility in materials at high temperature; the proposed experimental technique is interesting because physical mechanisms can be checked with particularly good accuracy at strain rates within ranges much wider than the rates usually obtained from a single machine and a single type of sample.

References

1. Genevois-Stasi J (1998) Etudes des proprietes mecaniques et metallurgiques de l'Inconel 625 au cours du vieillissement – Utilisation de l'essai de disques sous pression, PhD, Paris 6
2. Jouinot P, Gantchenko V (2006) Lois de comportement mecanique et endommagement de membranes sous pression de gaz, Proceedings of ITCT, Paris, France, November 2006
3. Ecole Nationale superieure des Mines de Saint Etienne. www.emse.fr/fr/transfert/sms/depscientifiques/cnrsessaisprod.html
4. Jouinot P, Gantchenko V, Inglebert G, Ricciuis J (2004) Material damage induced by environment and temperature and identification process. Proceedings of ECCOMAS 2004, Jyväskylä, Finland, July 2004
5. Publication Number SMC-027. www.specialmetals.com
6. Jouinot P, Gantchenko V (2005) Reduction of material life by hydrogen environments and/or thermal ageing. Proceedings of EUCASS, Moscow, Russia, July 2005
7. Hill R (1950) Philos Mag Ser. 7, 41(322):1133
8. Duncan JL (1965) Bull Mech Eng Educ 4:29
9. Aubin V, Quauaegebeur P, Degallaix S (2002) Yield surface behaviour under biaxial fatigue. Proceedings of 8th international fatigue congress, Stockhom, Sweden, June 2002
10. Mesrar R (1991) Comportement plastique des toles sous sollicitation biaxiale et analyse numerique de la mise en forme par gonflement hydraulique. PhD, Metz
11. Boualila A, Ayadi M, Zghal A, JendoubiI K (2002) Validation experimentale du modele de calcul en calotte spherique de plaques circulaires minces sous l'effet d'un gonflement hydraulique. Mecanique et Industries, March 2002
12. Manjoine MJ (1944) J Appl Mech A 211:11
13. Nadaï A (1950) Theory of flow and fracture solid. McGraw Hill, New York, p 915
14. Dowling AR, Harding J, Camprell JD (1970) J Inst Met 98:215
15. Maddin R, Pond R (1951) Met Prog 60:76
16. Poirier JP (1979) Montee des dislocations. Dislocations et deformation plastique, Les Editions de Physique, p 223
17. Lemaitre J, Chaboche JL (1988) Mecanique des materiaux solides, Ed Dunod, p 319
18. Bouajila W (2007) Modelling of launcher's combustion chambers. Proceedings of 58th IAC Congress, Hyderabad, India, September 2007
19. Lemaitre J, Chaboche JL (1988) Mecanique des materiaux solides, Ed Dunod, p 322
20. Francois D, Pineau A, Zaoui A (1993) Comportement mecanique des materiaux, Ed Hermes, p 47
21. Campbell JD, Fergusson WG (1970) Phil Mag 21:63